Proceedings of the Seminar for Arabian Studies 54 (2025): 247–262

The production of Bahlā Ware in the context of late Islamic Oman

Jelena Živković, José Cristobal Carvajal López, Irini Biezeveld & Stephanie Döpper

Summary
Among glazed Arabian Gulf wares, Bahlā Ware stands out as one of the most documented objects of consumption at sites in Oman, the UAE, Qatar, and Bahrain from the sixteenth to the early twentieth century. Previous scientific studies of Bahlā Ware from UAE and Qatar formed the basis for understanding its production technology and provenance, as well as the unique composition of its lead-barium glaze. This paper presents the new results of petrographic and chemical analyses of thirty-two Bahlā samples from Oman, contributing to a better understanding of the compositional variability of ceramics, the provenance of raw materials, and techniques used for the application of lead-barium glazes. The compositional match between samples of Bahlā Ware from Oman, the UAE, and Qatar reveals the exploitation of the same geological source of raw materials over several centuries. Previous research has associated this source with the ophiolitic geological formation in Oman. The results of chemical analysis of glazes confirmed that the Omani samples were also coated with a lead-barium glaze of the same type as reported for UAE and Qatar.

Keywords: Bahlā Ware, late Islamic ceramic production, provenance, lead-barium glaze

Introduction

Bahlā Ware is a major class of late Islamic glazed pottery local to the Gulf, with well-documented findings reported from Oman (Biezeveld & Düring 2020: 206; Döpper 2022: 161; Costa & Wilkinson 1987), the United Arab Emirates (Power 2015: 10–11; Živković et al. 2019), Qatar (Carvajal López et al. 2019; Carter 2011: 37; Petersen et al. 2010: 48; Bystron 2019: 43; Garlake 1978a: 174; 1978b: 167), Bahrain (Carter & Naranjo-Santana 2011: 90–91), and Iran (Priestman 2005: 269–270). This ware consists of bowls, dishes, and storage jars coated with monochrome glazes of brown, green, and yellow colours (Fig. 1), which were used for food consumption, transportation, and storage. Their wide distribution and significant quantities at urban, rural, coastal, and inland sites across the Gulf highlights their importance for archaeological interpretations of socio-economic networks between the sixteenth and early twentieth centuries. The provenance of Bahlā Ware has been a subject of long-lasting debate, with either Khunj in Iran or Bahlā in Oman being considered as centres of production (Kennet 2004: 54; Priestman 2005: 270; Whitcomb 1975: 129; Carter 2011: 37).

Recent studies of Bahlā Ware using archaeological science methods have shed new light on questions of provenance, production technology, and potting traditions in the Gulf (Živković et al. 2019; Carvajal López et al. 2019). The consistency of mineralogical compositions of Bahlā samples from al-Ain and Doha indicated a common origin of raw materials used for the production of this particular type of ceramic. Research showed that this source of calcareous raw materials lies in the zone of the ophiolitic geological formation in Oman, likely within the boundaries of the town of Bahlā (Živković et al. 2019: 4707). This result ruled out Khunj as a production centre, at least for Bahlā Ware used on the Arabian side of the Gulf.

Additionally, the study of technology used in the production of these vessels showed an unexpected complexity concerning the composition of their glazes. The Bahlā glaze is of a lead-barium type unknown elsewhere in the Islamic World (Živković et al. 2019: 4706). The key components of this glaze are lead and barium sulphates that were naturally mixed in minerals, and as such extracted for the glaze preparation. Not only is this a very specific process, but sulphidic minerals containing barium also have poor fluxing properties and their use in the glaze preparation often requires more energy. As other seemingly less complex glazing technologies, such as the use of lead oxides associated with monochrome lead glazes, were available at the time,

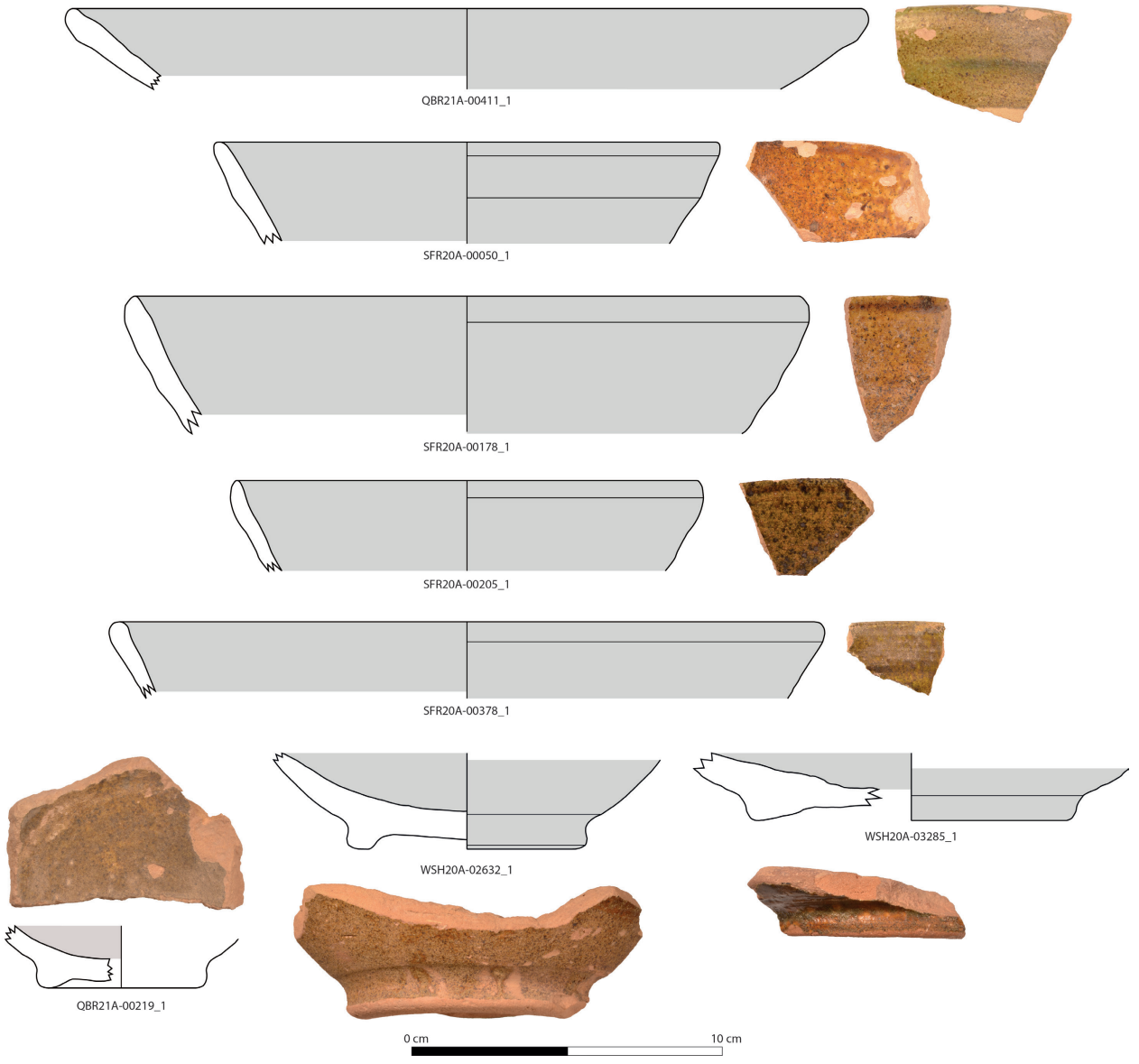

Figure 1. *Bahla Ware from Oman. Bowls: QBR21A-00411_1: surface find from Al-Qabrayn; SFR20A-00050_1, SFR20A-00178_1, and SFR20A-00378_1: surface finds from Safrat al-Khashbah; bases: QBR21A-00219_1: surface find from Al-Qabrayn; WSH20A-02632_1 and WSH20A-03285_1: surface finds from Al-Washhi.*

it is possible that the use of sulphidic minerals in glaze preparation was strongly embedded in the technological choices in producing Bahlā Ware, although we cannot pinpoint what the cultural significance of these choices were. Nevertheless, they were repeated and became a pattern of long-term exploitation of raw materials used for the production of both ceramic bodies and glazes, successfully transmitted as the know-how of a characteristic technological tradition within the Omani potting community.

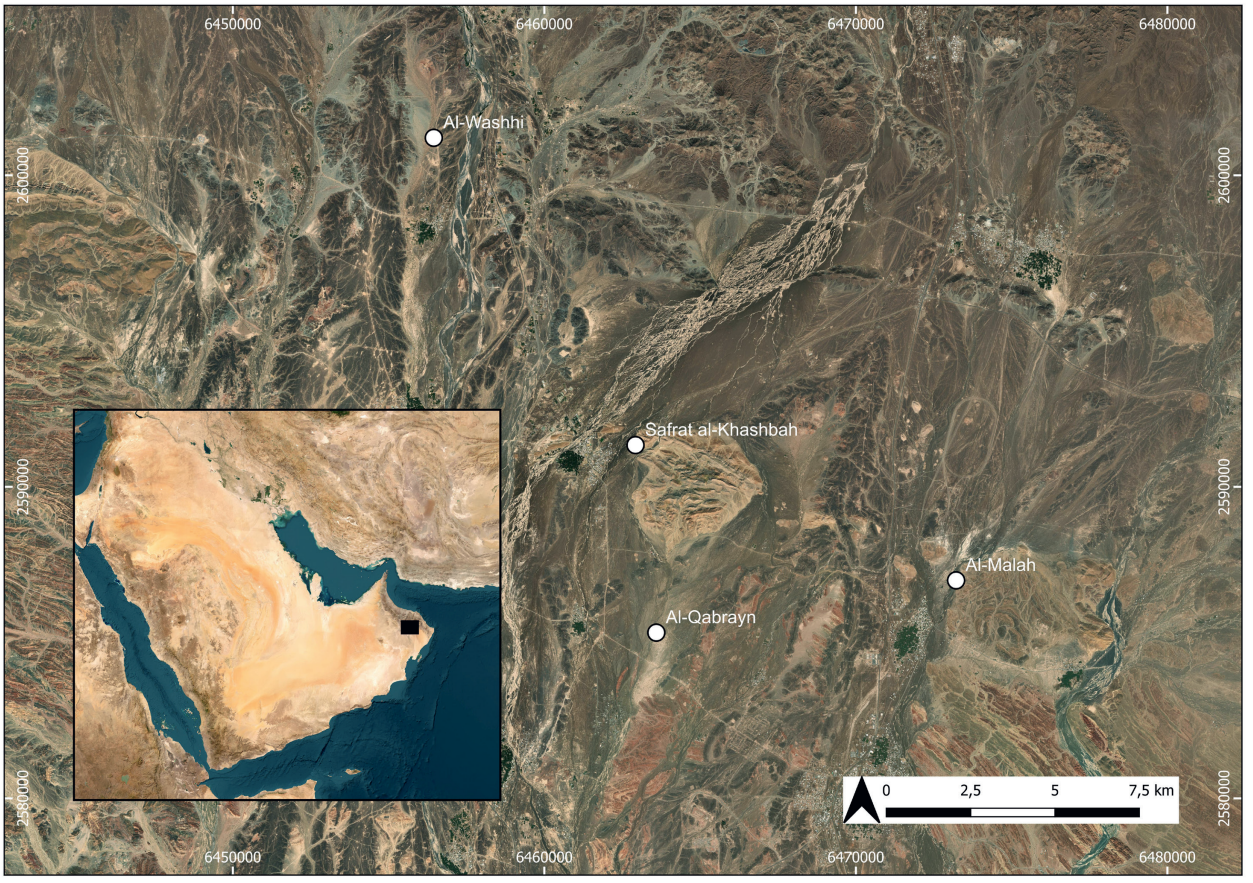

Figure 2. *A map showing the archaeological sites in Oman included in this study (basemap: ESRI).*

This study seeks to further characterize the production technology and knowledge of the provenance of Bahlā Ware by presenting the results of petrographic and chemical analyses of thirty-two samples of this ware recovered from rural settlements in northern Oman. The goal is to explore the compositional variability and investigate whether there are possible centres of production, other than those discussed in the context of the assemblages from al-Ain and Doha.

Archaeological background

As part of the project 'The abandoned mudbrick settlements of central Oman: between romanticization and neglect', funded within the Lost Cities framework of the Gerda Henkel Foundation, four late Islamic settlements — Al Malah, Safrat al-Khashbah, Al-Washhi, and Al-Qabrayn — were surveyed and partially excavated between 2020 and 2022 (Biezeveld 2023). They are all located in the Wilayat of Al-Mudhaybi in the governorate of Al-Sharqiyah North in the Sultanate of Oman (Fig. 2).

Al-Malah is a rectangular mud-brick settlement surrounded by a wall with a freestanding tower in the centre of the settlement. The tower has its entrance on the first floor, which is common in central Oman (Bonnenfant, Bonnenfant & al-Harthi 1997: 118). Al-Malah was described by the British traveller J.G. Lorimer (1908: 1767) as a deserted town with 600 date trees in the oasis. Radiocarbon dates from test trenches excavated at the site have yielded dates in the eighteenth and nineteenth centuries, with only

	Trench	Lab Code (MAMS)	Sample Name	14C Age [yr BP]	±	δ13C AMS [‰]	2σ cal. CE	Material
Al-Malah	1	56324	MLH22A-01008	111	18	-35.3	1691–1921	charcoal (Acacia)
	1	56325	MLH22A-01009	273	18	-29.7	1524–1792	palm mat
	2	56326	MLH22A-01017	131	17	-28.5	1682–1938	charcoal (indet.)
	2	56327	MLH22A-01022	98	17	-24.9	1694–1917	charcoal (indet.)
Safrat al-Khashbah	2	56328	SFR22A-00014	215	17	-32.2	1647–1950	charcoal (indet.)
	2	56329	SFR22A-00024	141	18	-31.9	1673–1944	charcoal (Acacia)
	3	56330	SFR22A-00056	140	18	-25.7	1674–1943	palm mat
	3	56331	SFR22A-00057	150	17	-29.3	1670–1950	charcoal (Acacia)
	3	56332	SFR22A-00064	162	17	-26.9	1667–1950	charcoal (Acacia or Prosopis)
Al-Washhi	2	56333	WSH22A-00028	224	19	-25.9	1642–1800	charcoal (Phoenix dactylifera stem)
	1	56334	WSH22A-00053	186	18	-29.9	1661–1950	date pit
	1	56335	WSH22A-00059	328	18	-29.6	1494–1638	charcoal (Acacia or Prosopis)
	2	56336	WSH22A-00064	246	18	-24.0	1639–1797	charcoal (Phoenix dactylifera)
Al-Qabrayn	1	56342	QBR22A-00072	130	18	-25.6	1682–1937	charcoal (indet.)
	1	56346	QBR22A-00158	215	18	-29.5	1647–1950	charcoal (Phoenix dactlyfera stem)
	1	56347	QBR22A-00169	131	20	-20.2	1680–1940	charcoal (Phoenix dactlyfera petrole)
	2	56348	QBR22A-00199	220	18	-26.5	1644–1945	date pit

Figure 3. *Radiocarbon dates from archaeological sites. The ^{14}C ages are calibrated to calendar ages using the IntCal20 data set and the Oxcal software. Charcoal was determined by L. Proctor.*

one exception dating back to the seventeenth century (Fig. 3). The archaeological finds, such as glass bangles and a late nineteenth-century coin minted by Sultan Faisal Bin Turkee fall within this dating range.

Safrat al-Khashbah was briefly described by Al-Jahwari (2008: 472, site CS.5.8) and Schmidt et al. (2021: 240–242). It is located 1 km from the modern-day village of Al-Khashbah and consists of twenty-five buildings and a large field system. Radiocarbon dates have a rather wide range, between the eighteenth and twentieth centuries (Fig. 3), as does the retrieved pottery, which includes Chinese Blue and White as well as modern coffee cups.

Al-Washhi is not as well preserved as the other sites; there are no mud-brick remains and only the foundations of the buildings can be seen. It thus seems likely that this site was abandoned in a period before the other sites. It lies 2.5 km north of the modern village of Al-Washhi and consists of ten buildings, including the foundations of a tower. Based on radiocarbon dating and finds collected during survey and excavation, the settlement was in use between the seventeenth and nineteenth centuries (Fig. 3). The whole area was covered with slag, indicating intensive copper processing.

Al-Qabrayn differs from the other sites in being a fort-like structure surrounded by a large field system, and a handful of scattered buildings in the field system. The fort consists of two towers that are located across from each other. The towers are equipped with shooting holes and the entrance was probably on the first floor,

as can be seen at other towers in the region. During the survey, various coins were collected, including a quarter Anna of the East India Company from AD 1832, as well as a coin from 1299 AH (AD 1881–1882). Radiocarbon dates are available from excavations in the fortified area, and their dates range between the seventeenth to eighteenth and the eighteenth to twentieth centuries (Fig. 3).

More than 6000 sherds were collected from both the excavation and the survey, with *c.*3700 diagnostic sherds from the survey and 325 diagnostic sherds from the excavations. The majority of these sherds are medium coarse and coarse ware with lower numbers of comb-impressed pottery, porcelain, and more than 500 Bahlā Ware sherds (409 from Al-Washhi, 97 from Al-Malah, 66 from Al-Qabrayn, and 48 from Safrat al-Khashbah). From the latter, thirty-two sherds (10 from excavation contexts, 22 surface material collected during the surveys) were chosen for scientific analysis. The selection favoured recognizable forms (rim and base sherds) and sherds from excavation contexts. It also aimed for an approximate equal distribution of the samples across the four sites (9 sherds from Al-Qabrayn, 8 sherds from Al-Malah, 8 sherds from Al-Washhi, and 7 sherds from Safrat al-Khashbah) (Fig. 4).

Methodology

The scientific analysis of ceramics carried out in this study consisted of three methods. Ceramic petrography and wavelength dispersive X-ray fluorescence (WD-XRF) analysis were used for the compositional characterization of ceramic bodies and their provenance determination. All thirty-two samples were subjected to petrographic analysis while a sub-set of twenty-eight samples was studied with WD-XRF analysis. Scanning electron microscopy with energy dispersive spectrometry (SEM-EDS) analysis was used for the characterization of chemical composition of glazes and their application methods. After obtaining the results from the petrographic and chemical analyses of the ceramics, a sub-set of fifteen samples containing well-preserved glazes of a range of colour tones and thickness were subjected to SEM-EDS analysis.

This methodology is compatible with that of previous scientific studies of Bahlā Ware from al-Ain (Živković et al. 2019) and Doha (Carvajal López et al. 2019), which enables the comparative analysis of production technology and provenance.

Ceramic petrography

Thin sections of the selected ceramics were prepared in the laboratories of the School of Archaeology and Ancient History at the University of Leicester, UK (the thin sections were then analysed on a microscope with a polarizer, a ZEISS AXIOSCOPE 5 POL, in the same laboratories). This analysis enables the identification of rocks and minerals, as well as patterns in the way in which they are grouped, and optical characteristics of the ceramic matrix in which they are embedded (all of which is known as 'texture'). All these elements are indicative of technological choices taken by the potter when selecting and mixing the clays ('clay recipes') and when firing them. The methodology of analysis and grouping of ceramic thin sections that was followed is well developed in the works of I. Whitbread (1995: 365–396; 2001) and P. Quinn (2022).

Elemental analysis of ceramics (WD-XRF)

Samples for the WD-XRF analysis of ceramics were submitted to the Fitch Laboratory of the British School at Athens. The analysis was carried out on a BRUKER S8 TIGER with a 4kW Rh X-ray tube instrument. The instrument measures twenty-six elements: Na, Mg, Al, Si, P, K, Ca, Ti, Fe, V, Cr, Mn, Co, Ni, Cu, Zn, Rb, Sr, Y, Zr, Ba, La, Ce, Nd, Pb, and Th. The custom calibration of the instrument was based on forty-three certified reference materials (for details see Georgakopoulou et al. 2017: 187). Two certified reference materials — CRMs: PMS and GSR-1 — were analysed together with the samples in order to monitor the instrument performance (Georgakopoulou et al. 2017).

Prior to pulverizing the samples and the preparation of glass beads, glazes were removed and the ceramic surface was cleaned with a tungsten-carbide drill. Glass beads were prepared as a mixture of 1 g of the pulverized and ignited sample and 6 g of a mixture of lithium metaborate/lithium tetraborate with lithium bromide as a non-wetting agent. Despite the cleaning, high contents of main elements found in glazes — Pb, Ba, and Cu — show the persistent contamination of

	Code FITCH	Code Thin Section	Label	Building	Room	Context	Unit	UTM WGS 84 40N East	UTM WGS 84 40N North
Al-Malah	MAL001	BAHIB 08	MLH22A-00328	MLH-0016	MLH-PD	surface	MLH-A-Fs0041	618150.61	2502710.75
	MAL002	BAHIB 26	MLH22A-00196	MLH-0009	MLH-IC	surface	MLH-A-Fs0027	618150.34	2502678.31
	MAL003	BAHIB 15	MLH22A-00454	MLH-0019	MLH-SB	surface	MLH-A-Fs0050	618156.58	2502735.93
	MAL004	BAHIB 21	MLH22A-01020	MLH-0016	MLH-PB	trench 2	MLH-A-Fs0087	618155.04	2502704.38
	MAL005	BAHIB 28	MLH22A-00335	MLH-0017	MLH-QA	surface	MLH-A-Fs0042	618148.91	2502704.43
	MAL006	BAHIB 32	MLH22A-00345	MLH-0017	MLH-QB	surface	MLH-A-Fs0043	618151.76	2502707.11
	MAL008	BAHIB 20	MLH22A-0103 (sorted from MLH22A-01019)	MLH-0016	MLH-PB	trench 2	MLH-A-Fs0087	0	0
	MAL008	BAHIB 27	MLH22A-0103 (sorted from MLH22A-01019)	MLH-0016	MLH-PB	trench 2	MLH-A-Fs0087	0	0
Safrat al-Khashbah	SFR001	BAHIB 09	SFR20A-00015	SFR-0001	SFR-AD	surface	SFR-A-Fs0004	608654.63	2506565.18
	SFR002	BAHIB 31	SFR20A-00205	SFR-0014	SFR-NB	surface	SFR-A-Fs0057	608665.64	2506634.57
	SFR003	BAHIB 17	SFR20A-00378	field system	-	surface	SFR-A-Fs0079	608473.75	2506512.41
	SFR004	BAHIB 25	SFR20A-00178	threshing platform	-	surface	SFR-A-Fs0048	608660.76	2506657.01
	SFR005	BAHIB 12	SFR20A-00050	SFR-0003	SFR-CB	surface	SFR-A-Fs0010	608653.78	2506583.11
	SFR006	BAHIB 22	SFR20A-00072	SFR-0004	SFR-DE	surface	SFR-A-Fs0018	608672.90	2506568.08
	SFR007	BAHIB 24	SFR20A-00071	SFR-0004	SFR-DE	surface	SFR-A-Fs0018	608672.48	2506569.63
Al-Washhi	WSH001	BAHIB 18	WSH20A-01906	WSH-0009	WSH-IC	surface	WSH-A-Fs0029	602605.57	2515632.33
	WSH002	BAHIB 19	WSH20A-01932	WSH-0009	WSH-ID	surface	WSH-A-Fs0030	602609.35	2515635.24
	WSH003	BAHIB 29	WSH20A-03209	WSH-0008	WSH-HH	surface	WSH-A-Fs0034	602609.61	2515627.27
	WSH004	BAHIB 05	WSH20A-02632	WSH-0010	WSH-JC	surface	WSH-A-Fs0040	602600.57	2515627.21
	WSH005	BAHIB 07	WSH20A-03285	WSH-0010	WSH-JI	surface	WSH-A-Fs0047	602603.81	2515634.09
	WSH006	BAHIB 30	WSH20A-00055	WSH-0002	WSH-BB	trench 1	WSH-A-Fs0003	602612.02	2515802.77
	WSH007	BAHIB 03	WSH22A-00066 (sorted from WSH20A-00047)	WSH-0002	WSH-BB	trench 1	WSH-A-Fs0003	602614.67	2515805.66
	WSH007	BAHIB 04	WSH22A-00066 (sorted from WSH20A-00047)	WSH-0002	WSH-BB	trench 1	WSH-A-Fs0003	602614.67	2515805.66
Al-Qabrayn	QAB001	BAHIB 13	QBR21A-00219	QBR-0001	QBR-AS	surface	QBR-A-Fs0017	609295.20	2501098.49
	QAB002	BAHIB 10	QBR21A-00009	QBR-0001	QBR-AB	surface	QBR-A-Fs0002	609297.15	2501113.23
	QAB003	BAHIB 06	QBR21A-00630	field system	-	surface	QBR-A-Fs0038	609316.41	2500747.90
	QAB004	BAHIB 11	QBR21A-00411	QBR-0006	QBR-FA	surface	QBR-A-Fs0026	609415.99	2500938.60
	QAB005	BAHIB 23	QBR21A-00228	QBR-0001	QBR-AS	surface	QBR-A-Fs0017	609292.10	2501100.57
	QBR001	BAHIB 14	QBR22A-00281 (sorted from QBR22A-00192)	QBR-0001	QBR-AI	trench 2	QBR-A-Fs0064	0	0
	QBR002	BAHIB 16	QBR22A-00279 (sorted from QBR22A-00022)	field system	-	surface	QBR-A-Fs0041	0	0
	QBR003	BAHIB 01	QBR22A-00280 (sorted from QBR22A-00056)	QBR-0001	QBR-AS QBR-AR	trench 1	QBR-A-Fs0055	0	0
	QBR003	BAHIB 02	QBR22A-00280 (sorted from QBR22A-00056)	QBR-0001	QBR-AS QBR-AR	trench 1	QBR-A-Fs0055	0	0

Figure 4. *A list of pottery samples and their find contexts.*

ceramic bodies caused by diffusion of these elements from the glaze (Živković et al. 2024: table CHEM 1). For the statistical treatment of WD-XRF data, therefore, these elements were excluded. Additionally, Th was excluded because the high concentrations of Pb affect its accuracy, as measured with the Fitch WD-XRF setup (Georgakopoulou et al. 2017). P_2O_5 was also disregarded because of its association with diagenetic contamination of ceramics (Freestone, Meeks & Middleton 1985).

A principal component analysis (PCA) was used to examine relationships between the twenty-one elements. The chemical data were transformed to logratios prior to the PCA.

Chemical analysis of glazes (SEM-EDS)

The SEM-EDS analysis of glazes was carried out at the Archaeological Science Laboratories of the Cyprus Institute. SEM instrument Zeiss EVO 15 that operates with an attached EDS (Oxford Instruments Ultim Max EDS with a 65 SSD detector) was used. The analysis was run in high vacuum conditions, at an accelerated voltage of 20 kV, working distance 8.50 mm, process time 4, and acquisition time 30s live time. The microstructure of glazes was studied using the backscatter image mode.

Corning Glass Standard C was analysed together with the archaeological samples to monitor the instrument's performance (Brill 1999: 542). The accuracy was measured in comparison to the recently published certified values of Corning glasses (Adlington 2017). The difference between the means of the certified values and those measured in this research (estimated as ((xcert – xmeas)/xmeas) x 100) were below 9.1% for Na_2O, MgO, Al_2O_3, SiO_2, K_2O, CaO, Fe_2O_3, CuO, Ba, and PbO, except for TiO_2 where it is 21.6% and CoO where it is 17.6%. The precision, estimated as relative standard deviation (RSD) is within 6.5% for the major elements. For TiO_2 and CoO, RSD is 17.6% and below.

Bahlā glazes are heterogeneous and for their study a case-specific methodology has been developed (see Živković et al. 2019). Clear areas of the glaze matrix were analysed using x800 magnification and area scans of *c.*135 x 45 µm that were selected in the middle of the glaze layer. In samples with completely crystallized glazes (BAHIB_05 and 24), the bulk compositional analysis included various inclusions. The same magnification and the size of area scans were used for glaze bulk analysis as for glaze matrix analysis. For some samples, both types of glaze compositional analyses were documented. Inclusions were separately analysed using spot analysis. The study of application methods required measurements of three additional areas. The bulk analysis of ceramic bodies was carried out using x300 magnification and area scans of 368 x 280 µm. The layer of glaze above the interface (glaze/low) was analysed using x800 magnification and area scans of *c.*50 x 15 µm. The layer of ceramic body below the interface (ceramic body/up) was analysed using x400 magnification and area scans of *c.*255 x 65 µm.

Results

The full set of results of the analysis discussed in this article can be consulted in the associated database (Živković et al. 2024).

The mineralogical and petrological composition of ceramics

The petrographic analysis of the samples indicates that they all belong to the same group (Figs 5 & 6), which is defined by several characteristics. One of them is an abundance of sedimentary components, mainly micritic limestone (as in Fig. 6/B and C) and clay pellets (as in Fig. 6/A and C). They also include a component of mafic and ultramafic detritic rocks, some of them metamorphosed to serpentinite (Fig. 6/A–D). The other element is the texture of the matrix, which is slightly inhomogeneous and with a level of optical activity that indicates a relatively stable maximum firing temperature reached across all the samples (examples of this inhomogeneity and variation in the matrix can be seen in Fig. 6/A–D). This fabric matches very well the composition of the Limestone and Serpentinite Fabric of the Bahlā Ware from al-Ain (Živković et al. 2019) and Fabric 7 from Doha (Carvajal López et al. 2019). Of these two, the former contains inclusions consistent with the geological composition of the ophiolitic mountain in Oman, including those found around the town of Bahlā, home to ceramic production workshops in the past (Živković et al. 2019: 4707). Fabric 7 in Doha is considered essentially the same in terms of composition and provenance. This is also the case with the fabric described in this paper. The geological

Fabric name (unique)	Textural characteristics	Main inclusions	Technological implications
Limestone-rich sedimentary fabric with serpentinite	Low number of pores (1–5%) and abundant inclusions (20–40%). Poorly sorted (close- to single-spaced in some samples, open-spaced in others), weakly to moderately aligned inclusions, unimodal grain-size distribution.	TF1 (clay pellet) (Predominant-Common, high to neutral optical density; <3.6 mm); micritic limestone (Dominant-Common; <1.4 mm); TF2 (calci-mudstone) (Frequent-Common, diffuse boundaries, low optical density; <2 mm). Other inclusions in the coarse fraction include serpentinite (Few), pyroxene, serpentinised amphibole (Very Few) and recrystallised quartzite (Very Rare). In the fine fraction there is monocrystalline quartz and micritic limestone (Dominant-Common), serpentinite and birefringent minerals (Common-Few), plagioclase feldspar and chert (Few) and amphibole (Very Few).	The wide variability of the fabric in the abundance of inclusions in its fine fraction and in the abundance of limestone and TFs suggests that the fabric was produced in a range of workshops in a same area and with the same basic technical traits over a period of time, rather than of a single workshop well localized in time. The mafic rocks documented are detrital in a sedimentary deposit from which the clay was collected. The elements of the fine fraction are abundant enough to suggest that there is no levigation process. The relatively relevant appearance of TFs suggests a possibility of clay mixing, in particular of a purer darker clay that would form the clay pellets and twirls, but more experiments would be required to test this (it must be noted that if there is clay mixing, then the recipe would include only a very small part of the purer clay). The lack of widespread optical activity suggests a high equivalent temperature of firing, and the similarities of the colours of the matrix suggest a very uniform atmosphere. All this speaks again of a very standardized way of production.

Figure 5. *Description of the petrographic fabric identified in the assemblage studied in this paper. This is a simplified version of the fabric description published on the online database by Živković et al. (2024: Petrographic fabric document).*

background (which includes fragments of ophiolites) is the same for all. It is true that some minor differences can be noted between the descriptions, but these point mainly to possible variations in the technological process of manufacturing, which may be caused by the technological choices of different artisans. Among the variations noted, there are wide ranges of the frequency of inclusions across different samples, which may indicate the use of different quarries or slightly different clay recipes. The relative abundance of clay pellets in some samples could be interpreted as clay mixing in some cases, but there is no definite evidence to support the use of this technological process at this stage. To be sure, the observed variation does not show regular patterns on which sub-categories or groups can be made. For this reason, in the present analysis the fabric has been maintained as a single group until more samples of Bahlā Ware and more targeted analysis can be undertaken. In the future, the potential different technical choices should be explored to determine if they are significant enough to define different fabrics or sub-fabrics to be considered under the term 'Bahlā Ware'.

The chemical composition of ceramics

The results of WD-XRF analysis show that all samples of Bahlā Ware from Oman form a single chemical cluster, suggesting a common origin of raw materials used for its production (Živković et al. 2024). This is calcareous pottery characterized by varying contents of CaO (5.6–17.8 wt%), which is related to the uneven distribution of limestone as observed by petrography. Among trace elements, a relatively high variability is measured for Sr (229–660 ppm), Cr (423–718 ppm), and Mn (392–690 ppm). Sr is related to CaO in calcareous ceramics while Cr can be associated with serpentinite (Quinn 2022: 387), which is another rock identified petrographically. The variability of these elements can therefore be explained by the natural heterogeneity of raw materials.

The PCA plot shown in Figure 7 illustrates the matching compositions of Bahlā ceramics from Oman

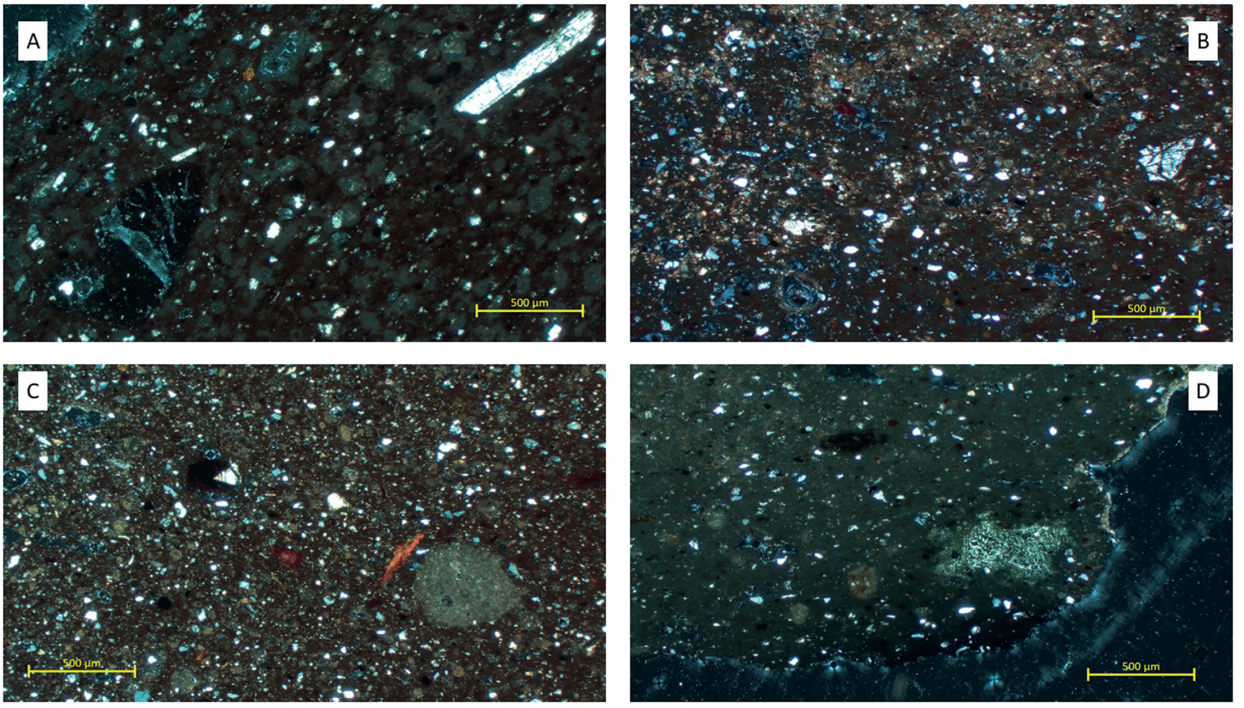

Figure 6. *Microphotographs of several samples, all in crossed polars.* **A.** *Sample 1, showing a burnt clay pellet on the lower left side and a birefringent mineral, probably a serpentinized amphibole, in the upper right corner;* **B.** *Sample 13, showing a more calcareous matrix with micritic limestone and quartz in the fine fraction. To the right of the image a serpentinized amphibole is very clear;* **C.** *Sample 7, showing a very calcareous matrix over which a larger grain of micritic limestone (centre right) and a burnt clay pellet (centre left, slightly towards the top) can be seen. Between them there are some orange fragments of serpentinite;* **D.** *Sample 20, showing a relatively clean matrix with some TFs and a relatively large fragment of a serpentinized mafic rock (images taken from the online database published by Živković et al. (2024: Petrography micro-images).*

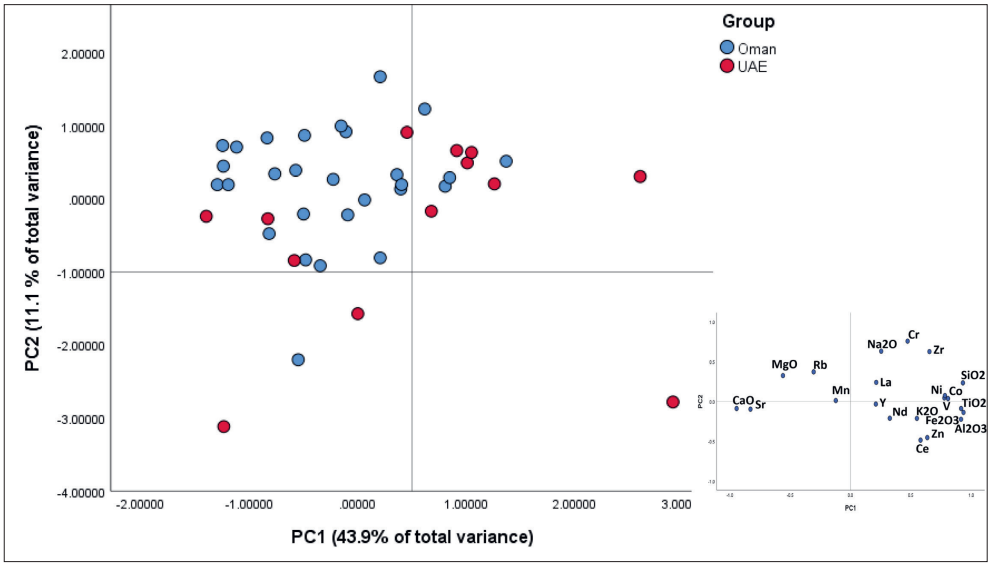

Figure 7. *Scatter-plot of the first two principal components and plot of loadings derived from principal component analysis of the WD-XRF elemental data treated as log ratios, showing all Bahlā samples from Oman and the C1 cluster of Bahlā samples from al-Ain (Živković et al. 2019: 4703). Excluded elements are P_2O_5, Cu, Ba, Pb, and Th.*

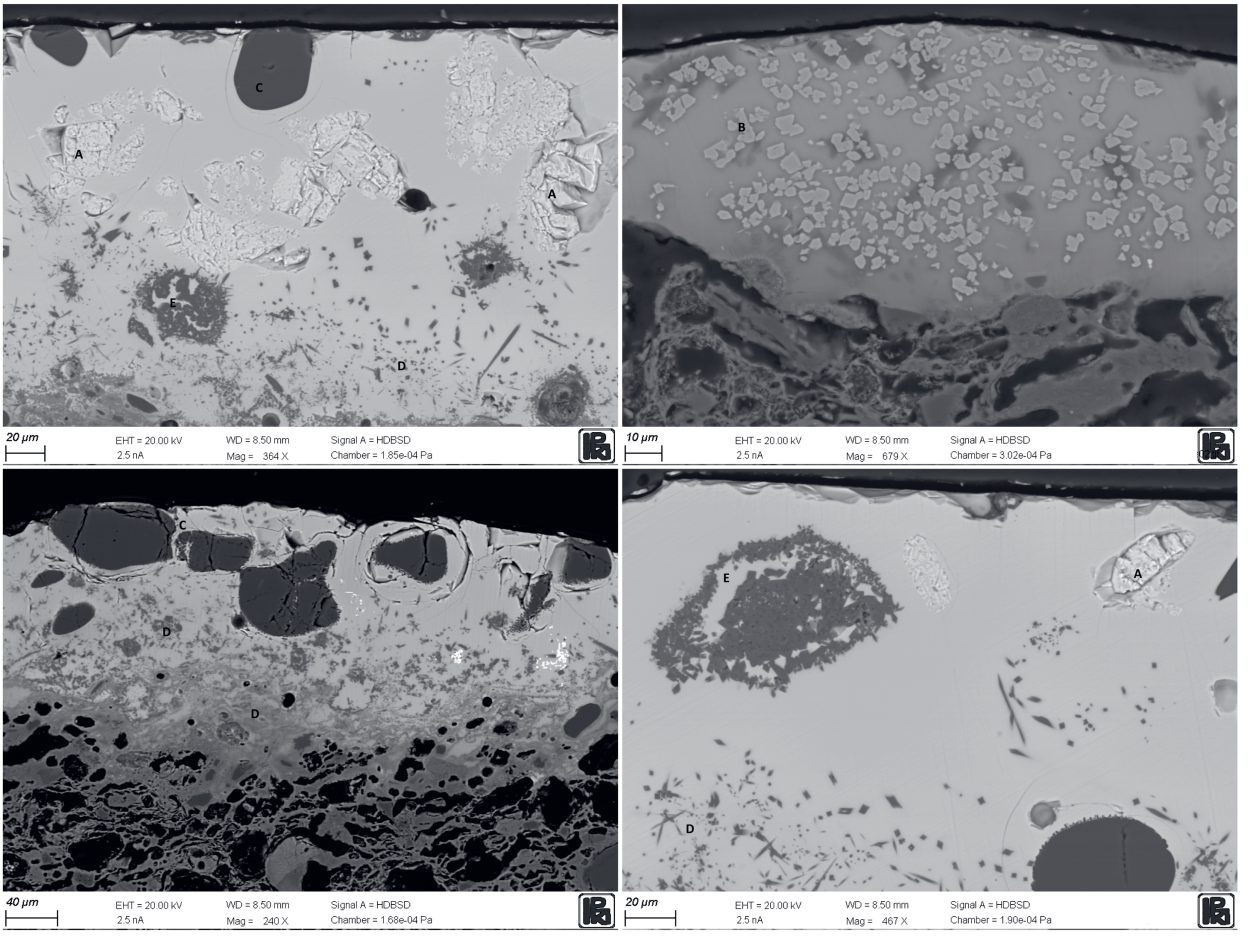

Figure 8. *SEM photomicrographs of Bahlā lead-barium glazes taken in the backscatter mode. Visible inclusions are non-dissolved baryte (A), iron oxides (B), quartz (C), crystals of the ceramic-glaze interface (D), and Ca-rich pyroxenes floating in the glaze (E). Top left BAHIB_04; top right BAHIB_15; bottom left BAHIB_09; bottom right BAHIB_04 (images taken from the online database published by Živković et al. [2024: SEM-EDS figures]).*

and the C1 cluster of Bahlā ceramics from al-Ain (Živković et al. 2019: 4702–4703). Comparisons with samples from Doha are not possible here because chemical data from that site have not yet been published. Two samples from al-Ain — B114 and B195 — visible on the right side of the PCA plot, stand out because of the lower content of CaO and the variability of several trace elements related to it, as explained by Živković et al. (2019: 4703). In both groups, the variability of CaO, Sr, Cr, and Mn is observed, which can be taken as a characteristic of raw materials used for the production of Bahlā Ware.

The chemical composition of glazes

The SEM photomicrographs show that the thickness of Bahlā glazes varies between 80 and 250 µm (Fig. 8). The glaze layer contains various inclusions. The most common are those of non-dissolved barium-sulphate or baryte ($BaSO_4$) that ranges in size from small (2 x 9 µm) to large (50 x 25 µm) sub-angular lumps, both easily identifiable by their bright colours in the backscattered mode (Fig. 8/A). They have a scattered distribution throughout the glaze layer. Another type of bright-colour

Sample		Na_2O	MgO	Al_2O_3	SiO_2	K_2O	CaO	TiO_2	FeO	NiO	CuO	BaO	PbO
BAHIB_02 (5)	mean	1.5	0.8	1.2	56.1	5.4	3.2	–	14.1	–	–	12.5	5.1
	stand. dev.	0.1	0.1	0.1	1.4	0.2	0.3	–	1.7	–	–	1.0	0.3
BAHIB_04 (5), interior	mean	0.6	1.4	2.5	43.6	1.3	3.1	–	5.1	–	–	4.7	37.8
	stand. dev.	–	–	0.2	1.0	0.1	0.2	–	0.2	–	–	0.4	0.5
BAHIB_04 (4), exterior	mean	0.6	1.9	2.7	44.5	1.5	3.6	–	5.4	0.8	–	4.8	34.2
	stand. dev.	0.0	0.2	0.1	1.3	0.1	0.3	–	0.2	0.2	–	2.1	0.7
BAHIB_06 (5), interior	mean	2.8	1.9	2.5	52.0	6.3	3.1	–	13.1	–	–	16.3	2.2
	stand. dev.	0.1	0.2	0.3	1.0	0.1	0.3	–	1.2	–	–	1.0	0.2
BAHIB_06 (4), exterior	mean	1.7	1.6	2.7	45.2	4.5	3.1	–	11.1	–	0.2	11.5	18.5
	stand. dev.	0.2	–	0.1	1.0	0.2	0.1	–	0.4	–	–	0.3	0.5
BAHIB_08 (5)	mean	1.3	1.6	2.7	52.9	2.0	5.6	–	10.9	–	–	20.9	2.1
	stand. dev.	0.1	–	0.3	0.6	0.1	0.3	–	0.5	–	–	0.3	0.1
BAHIB_09 (5)	mean	0.9	2.0	2.6	51.1	1.6	6.1	–	6.4	–	0.9	20.9	7.5
	stand. dev.	0.1	0.1	0.1	1.0	0.1	0.3	–	0.3	–	0.2	1.0	0.4
BAHIB_10 (5)	mean	1.6	1.0	1.2	54.1	5.0	1.8	–	13.0	–	0.5	13.0	8.9
	stand. dev.	0.1	0.1	0.3	2.8	0.5	0.3	–	1.5	–	0.1	1.6	0.8
BAHIB_11 (6), interior	mean	1.8	1.3	1.2	54.9	3.8	3.6	–	10.7	–	2.1	14.4	6.2
	stand. dev.	0.1	0.1	0.1	1.1	0.3	0.4	–	0.6	–	0.2	1.0	0.1
BAHIB_11 (3), exterior	mean	1.5	1.3	1.5	55.1	3.5	3.1	–	10.8	–	1.2	14.4	7.7
	stand. dev.	0.1	0.1	–	3.1	0.2	0.3	–	1.7	–	0.1	1.0	0.6
BAHIB_12 (5)	mean	1.8	1.3	1.4	51.4	4.2	4.0	–	15.8	–	0.2	18.2	1.8
	stand. dev.	0.1	0.1	0.1	0.9	0.1	0.1	–	0.8	–	–	0.4	–
BAHIB_14 (5)	mean	0.2	0.9	1.8	34.0	0.5	2.3	–	4.6	–	–	3.7	52.1
	stand. dev.	–	–	0.2	0.4	0.0	0.1	–	0.1	–	–	0.1	0.5
BAHIB_15 (5)	mean	1.5	1.1	1.4	56.4	4.7	3.7	–	13.4	–	–	9.4	8.5
	stand. dev.	0.1	0.1	0.3	1.5	0.7	0.9	–	1.5	–	–	2.0	0.7
BAHIB_25 (5), interior	mean	1.8	0.8	1.1	54.9	4.5	2.6	–	13.0	–	0.4	15.2	5.8
	stand. dev.	0.1	0.1	0.3	2.0	0.3	0.6	–	1.9	–	–	1.0	0.3
BAHIB_25 (3), exterior	mean	2.0	1.3	1.3	54.4	5.5	3.5	–	11.8	–	0.4	14.2	5.6
	stand. dev.	–	0.1	0.3	1.4	0.3	0.4	–	0.4	–	–	1.0	0.3
BAHIB_26 (5)	mean	2.8	1.8	2.4	50.8	4.8	6.4	–	12.9	–	–	16.2	1.8
	stand. dev.	0.1	0.1	0.3	1.1	0.2	0.4	–	0.5	–	–	0.4	0.1
BAHIB_28 (5), interior	mean	1.9	1.8	1.9	58.4	4.8	5.4	0.4	11.7	–	–	12.9	0.8
	stand. dev.	0.1	–	0.3	0.6	0.1	0.5	–	0.8	–	–	0.2	0.1
BAHIB_28 (3), exterior	mean	2.2	1.5	2.4	57.7	4.7	6.4	0.5	10.6	–	–	13.4	0.6
	stand. dev.	–	0.2	0.4	0.8	0.1	0.3	–	0.9	–	–	0.6	0.1
BAHIB_29 (5)	mean	0.6	0.7	1.2	38.5	3.0	2.9	–	11.3	–	–	5.7	36.1
	stand. dev.	–	–	0.1	1.1	0.2	0.3	–	0.8	–	–	0.4	0.8
BAHIB_32 (5)	mean	1.7	1.6	2.0	57.6	3.2	4.6	–	11.6	–	–	16.4	1.3
	stand. dev.	–	–	0.1	0.7	0.1	0.1	–	0.8	–	–	0.4	0.1

Figure 9. *The chemical composition of glaze matrices (areas without inclusions) determined through SEM-EDS. The number in parenthesis denotes the number of area measurements taken on the SEM-EDS for each sample. All values are normalized to 100 wt%; '–' stands for below detection limits (table taken from the online database published by Živković et al. [2024: table SEM 1]).*

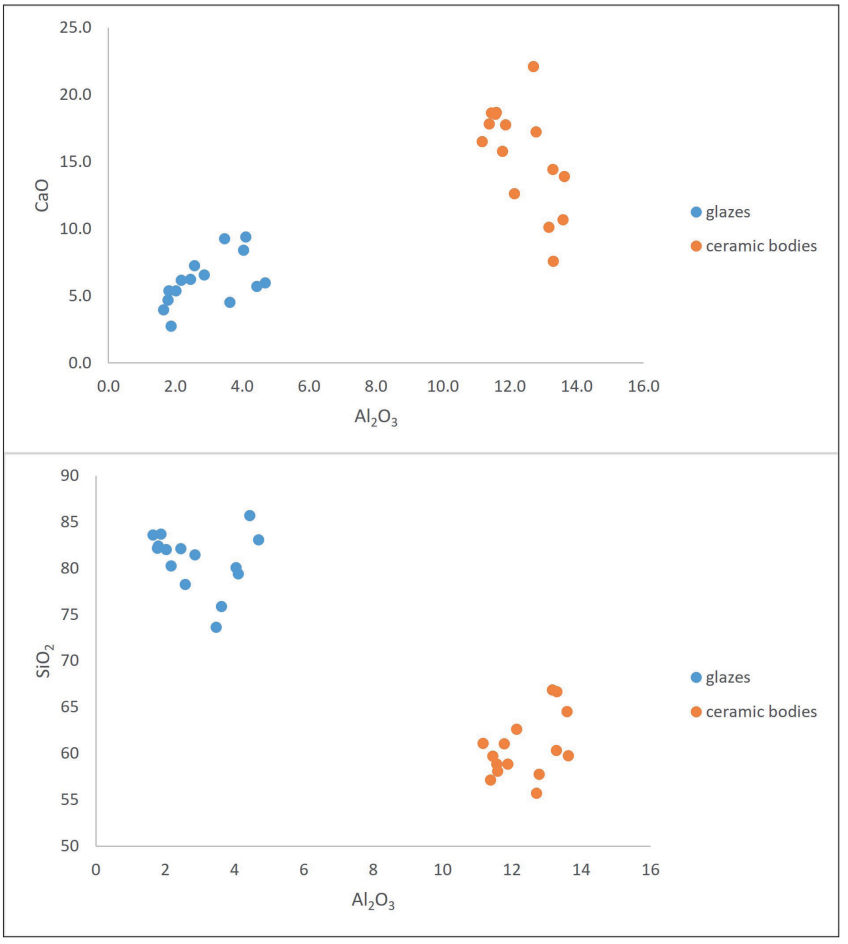

Figure 10. *Scatter plot showing the comparison between glazes and ceramic bodies of Bahlā Ware based on the chemical compositions determined through SEM-EDS. Excluded oxides are PbO, BaO, CuO, and FeO and remaining compositions were normalized to 100 wt%.*

inclusion is non-dissolved iron oxide (FeO is > 96 wt%) that was used for colouring the glaze (Fig. 8/B). These inclusions have rounded to sub-rounded shapes (*c.*5 x 5 µm) and appear densely clustered. Furthermore, coarse inclusions of quartz (max. 70 x 50 µm) are randomly scattered through the glaze (Fig. 8/C). A crystalline phase formed at the ceramic-glaze interface in some cases extends to include all layers of the glaze (Fig. 8/D). It is characterized by dark-colour inclusions of sub-angular shapes (*c.*3 x 3 µm) that are clustered together and appear floating in the glaze (Fig. 8/E). Compositionally, these are Ca-rich pyroxenes ranging between diopside ($CaMgSi_2O_6$) and hedenbergite ($CaFeSi_2O_6$), as already described by Živković et al. (2019: 4703).

Bahlā glazes are of the lead-barium type (Fig. 9). Looking at values measured for the glaze matrix, Bahlā glazes are characterized by a negative correlation between lead oxide, PbO (0.6–52.1 wt%) and barium oxide, BaO (3.7–20.9 wt%), which shows their natural mineralogical association. Glazes also contain varying contents of silica, SiO_2 (34.0–58.4 wt%), calcium oxide, CaO (1.8–6.4 wt%), sodium oxide, Na_2O (0.2–2.8 wt%), and potassium oxide, K_2O (0.5–6.3 wt%). More consistent values were observed for magnesia, MgO (0.7–2.0 wt%) and alumina, Al_2O_3 (1.1–2.7 wt%). The main colourant is iron oxide, FeO (4.6–15.8 wt%), that was deliberately added and, in some cases, not entirely dissolved in the glaze (BAHIB_02, 12, 15, 25). Green glazes also show the presence of copper oxide, CuO (0.2–2.1 wt%).

For the reconstruction of the glaze application methods, elements associated with glazes — PbO, BaO, CuO, and FeO — were excluded and the remaining composition was normalized to 100 wt% for the comparison with the ceramic body (as explained by Tite et al. 1998: 249–250). FeO was also excluded from the ceramic body composition because its value in the glaze

Sample	Area of analysis	Na_2O	MgO	Al_2O_3	SiO_2	K_2O	CaO	TiO_2	FeO	CuO	BaO	PbO
BAHIB_02	glaze/middle/matrix	1.5	0.8	1.2	56.1	5.4	3.2	–	14.1	–	12.5	5.1
	glaze/low/matrix	1.4	0.8	3.1	58.6	6.0	2.6	–	12.7	–	10.1	4.6
	c. body/up	0.7	6.3	11.5	51.6	2.1	22.3	0.8	4.8	–	–	–
	c. body/middle	1.1	6.2	10.9	56.6	1.8	17.7	0.6	5.2	–	–	–
BAHIB_04	glaze/middle/matrix	0.6	1.4	2.5	43.6	1.3	3.1	–	5.1	–	4.7	37.8
	glaze/bulk	0.6	2.2	4.3	45.4	1.6	5.3	–	4.9	–	4.6	31.0
	c. body/up	1.4	6.0	12.8	59.8	2.7	7.8	0.8	6.1	–	–	2.4
	c. body/middle	1.4	6.3	12.8	60.7	2.2	10.0	0.7	6.0	–	–	–
BAHIB_12	glaze/middle/matrix	1.8	1.3	1.4	51.4	4.2	4.0	–	15.8	0.2	18.2	1.8
	glaze/low/matrix	1.6	1.3	2.9	53.6	5.4	3.3	–	14.2	0.2	16.0	1.6
	interface	1.5	3.4	5.4	59.4	5.6	6.5	0.4	9.3	–	7.6	0.8
	c. body/up	0.9	7.2	12.9	53.9	3.0	15.7	0.6	5.7	–	–	–
	c. body/middle	1.0	7.6	11.1	57.6	1.6	14.9	0.6	5.7	–	–	–

Figure 11. *The chemical composition of different layers of samples determined through SEM-EDS, showing the gradual diffusion of elements. 'Glaze/middle' stands for the middle part of the glaze layer; 'glaze/low' for the layer of glaze located above the interface ('interface' refers to the ceramic-glaze interface); 'c. body/up' for the layer of ceramic body situated below the interface; and 'c. body/middle' for the middle part of the ceramic body. All values are normalized to 100 wt%; '–' indicates below detection limits (table taken from the online database published by Živković et al. [2024: table SEM 4]).*

is higher than in the body. The remaining compositions of ceramic bodies were also normalized to 100 wt%. The consistent differences between the composition of the glazes and the ceramic bodies suggest that the glaze recipe included the mixture of lead/barium compound and silica (Fig. 10).

The methodology used for studying firing methods of lead glazes proposed by Tite et al. (1998) and Molera et al. (2001) cannot be applied with certainty in this case, because the reaction between barium and lead in relation to archaeological ceramics is yet to be fully understood through laboratory experiments. However, some observations, indicative of the reaction between the ceramic body and the glaze during the firing process, can be outlined. First, the thickness of the ceramic-glaze interface varies significantly across the analysed assemblage. Some samples (BAHIB_06, 10, 11, 15, 25) have no visible interface while others (BAHIB_04, 05, 08, 09, 24, 26) have a thick one that covers approximately half of the glaze layer or more (see Fig. 8). While the former is more indicative of double-firing, the latter is associated with a single-firing regime, but this also depends on the cooling rates and the composition of the ceramic body (Molera et al. 2001: 1126–1127). Furthermore, when high-lead glazes are applied over raw calcareous ceramic bodies, the reaction results in the creation of Ca-rich pyroxenes in the glaze that appear to float away from the interface (2001: 1126). These crystallites are detected in the Bahlā glaze, as described above.

Another parameter to be considered is the diffusion of elements from the glaze (Pb/Ba) to the ceramic body and from the ceramic body to the glaze (Al, K, Ca). In all cases, PbO and BaO show a gradual decrease of values as measured from the middle to the lower part of the glaze layer located above the interface (Fig. 11). In only three samples, PbO is detected in the upper part of the ceramic body, situated below the interface (0.9–2.4 wt%), while the same can be said for BaO in one case only (0.2 wt%). Looking at a reverse pattern of diffusion, the content of Al_2O_3 is consistent in layers of middle and upper ceramic body, but then gradually drops in the lower part and the middle part of the glaze. Alkalis

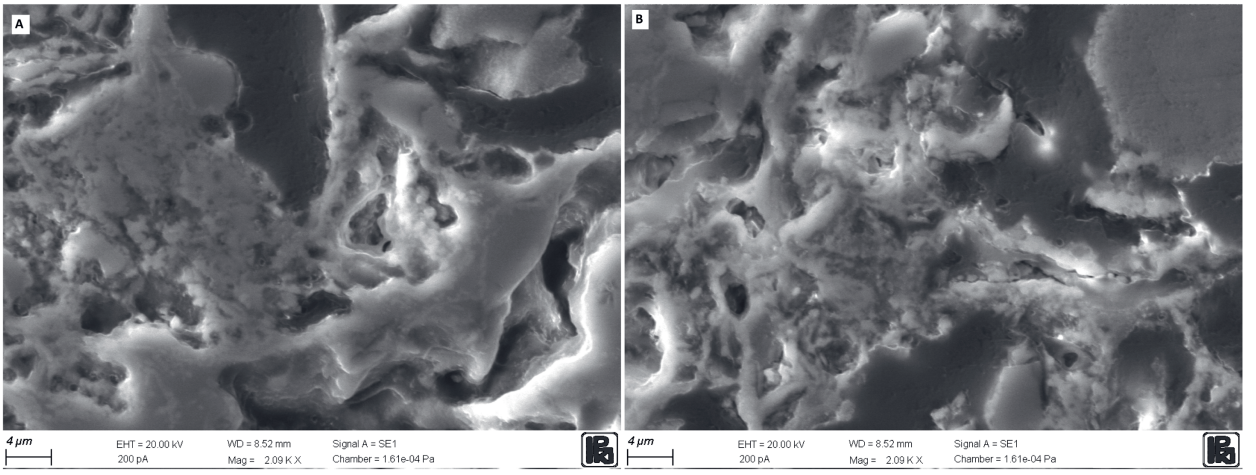

Figure 12. *SEM photomicrographs taken in the scanning electron mode of lead-barium glazes showing initial vitrification and areas of more extensive vitrification. Both A and B belong to BAHIB_08 (images taken from the online database published by Živković et al. [2024: SEM-EDS figs]).*

(Na_2O+K_2O) do not follow this pattern; their contents vary across different layers.

The gradual diffusion of elements and the scarce presence of PbO in the upper part of the ceramic body are indicative of double firing. This interpretation could be supported by the lack of the ceramic-glaze interface in several samples. On the other hand, the appearance of crystalline phases, both at the interface and Ca-rich pyroxenes in the glaze, would support the single-firing regime for many of the analysed samples.

The high-resolution SEM images, taken in the secondary electron mode, were also used for the study of ceramic body vitrification, which is indicative of approximate firing temperature (Quinn 2022: 409). The results show initial vitrification accompanied by areas of extensive vitrification, which is consistent with an approximate firing temperature range between 750 and 800°C (Fig. 12). This is in line with the petrographic observation of the matrix activity.

Discussion

This analysis of Bahlā Ware samples recovered from multiple sites in Oman confirms that their provenance is the same as those from assemblages in al-Ain and Doha, and is indicative of the spread of this important late Islamic pottery type. Raw materials used for the production of Bahlā Ware found at sites in the Oman peninsula and Qatar came from one source exploited in the range of the ophiolitic mountain. The production centre was probably in the town of Bahlā, but this is yet to be confirmed through a comparison between samples of archaeological pottery, kiln wasters, and geological clays.

Both petrographic and chemical data show that Omani samples are consistent with the Limestone Serpentinite fabric from al-Ain and all Bahlā samples from Doha. The variability observed in al-Ain's eighteenth-century assemblage, in which a few samples were described as outliers that have different compositions of ceramic bodies and glazes (Živković et al. 2019), was not attested in Oman. This variability therefore remains to be further investigated in the future.

The results of this study confirm the existence of a distinct technological tradition of pottery making in late Islamic Oman. This tradition is defined by the consistency in the exploitation of calcareous clays and the preparation of lead-barium glaze from sulphidic minerals, suggesting the successful transmission of this technical knowledge and skills from one generation of potters to the next. The workshop or workshops that produced Bahlā Ware played an important role in the regional trade network for several centuries.

Acknowledgements

This paper is dedicated to the memory of Myrto Georgakopoulou (1976–2022), a beloved colleague and friend. She was an invaluable member of the teams working on the scientific analysis of Bahlā Ware from al-Ain and Doha and had planned to contribute to this study of Omani samples. Although illness cut short her work, we remain deeply grateful for her expertise.

The archaeological fieldwork from which the sherds were analysed was made possible by funding from the Gerda Henkel Foundation (AZ 05/LC/19) under the Lost Cities framework. We are grateful to the School of Archaeology and Ancient History of the University of Leicester for infrastructural support; the A.G. Leventis Foundation for funding the glaze analysis; Noémi Müller, Evangelia Kiriatzi, and Zoe Zgouleta for the chemical analyses conducted at the Fitch Laboratories of the British School at Athens; Thilo Rehren for his support in the use of the SEM-EDS instrument at the Archaeological Science Laboratories of the Cyprus Institute; Judith López Aceves for the preparation of thin sections at the University of Leicester; and Giulia Fogarizzu for the preparation of polished blocks at the Cyprus Institute.

References

Adlington L.W. 2017. The Corning archaeological reference glasses: New values for 'old' compositions. *Papers from the Institute of Archaeology* 27/1: 1–8.

Biezeveld I. 2023. Re(dis)covering the recent: Surveying settlements and society in central Oman from the 17th to the 20th centuries. *Arabian Archaeology and Epigraphy* 34/S1: S107–S121.

Biezeveld I. & Düring B.S. 2020. Pre-oil globalization in a rural community: The late Islamic village of Sahlat in the Suhar Region. *Journal of Islamic Archaeology* 7/2: 199–219.

Bonnenfant P., Bonnenfant G. & al-Harthi S.H. 1997. Architecture and social history at Mudayrib. *Journal of Oman Studies* 3: 107–135.

Brill R. 1999. *Chemical analysis of early glasses.* ii. *Tables of analyses*. New York: The Corning Museum of Glass.

Bystron A.M. 2019. Pottery from al-Zubārah, Qatar: Reference collection and ware typology. *Proceedings of the Seminar for Arabian Studies* 49: 33–50.

Carter R. 2011. *Ceramics of the Qatar National Museum. Report on behalf of the Qatar Museums Authority*. Oxford: Oxford Brookes University.

Carter R. & Naranjo-Santana J. 2011. *Muharraq Excavations 2010*. Oxford: Oxford Brookes Archaeology and Heritage.

Carvajal López J.C., Giobbe M., Adeyemo E., Georgakopoulou M., Carter R. … al-Na'īmī F. 2019. Production and provenance of Gulf wares unearthed in the Old Doha Rescue Excavations Project. *Proceedings of the Seminar for Arabian Studies* 49: 51–67.

Costa P.M. & Wilkinson T.J. 1987. The hinterland of Sohar. Archaeological surveys and excavations within the region of an Omani seafaring city. *Journal of Oman Studies* 9: 1–238.

Döpper S. 2022. Walk the line: The 2020 field season of the al-Mudhaybi Regional Survey. *Proceedings of the Seminar for Arabian Studies* 51: 157–167.

Freestone I.C., Meeks N.D. & Middleton A.P. 1985. Retention of phosphate in buried ceramics: An electron microbeam approach. *Archaeometry* 27/2: 161–177.

Garlake P.S. 1978a. Fieldwork at al-Huwailah, Site 23. Pages 172–189 in B. de Cardi (ed.), *Qatar Archaeological Report. Excavations 1973*. Oxford: Oxford University Press.

Garlake P.S. 1978b. An encampment of the seventeenth to nineteenth centuries on Ras Abaruk, Site 5. Pages 164–171 in B. de Cardi (ed.), *Qatar Archaeological Report. Excavations 1973*. Oxford: Oxford University Press.

Georgakopoulou M., Hein A., Müller N. & Kiriatzi E. 2017. Development and calibration of a WDXRF routine applied to provenance studies on archaeological ceramics. *X-Ray Spectrometry* 46/3: 186–199.

Al-Jahwari N.S. 2008. Settlement patterns, development and cultural change in northern Oman peninsula: A multi-tiered approach to the analysis of long-term settlement trends. PhD thesis, Durham University. [Unpublished.]

Kennet D. 2004. *Sasanian and Islamic pottery from Ras al-Khaimah. Classification, chronology and analysis of trade in the western Indian Ocean.* Oxford: Archaeopress.

Lorimer J.G. 1908. *Gazetteer of the Persian Gulf.* ii. *Geographical and statistical*. London: British Library.

Molera J., Pradell T., Salvado N. & Vendrell-Saz M. 2001. Interactions between clay bodies and lead glazes. *Journal of the American Ceramic Society* 84/5: 1120–1128.

Petersen A., Grey T., Rees C. & Edwards I. 2010. Excavations and survey at al-Ruwayḍah, a late Islamic site in northern Qatar. *Proceedings of the Seminar for Arabian Studies* 40: 41–53.

Power T. 2015. A first ceramic chronology for the late Islamic Arabian Gulf. *Journal of Islamic Archaeology* 2/1: 1–33.

Priestman S.M.N. 2005. Settlement and ceramics in southern Iran: An analysis of the Sasanian and Islamic periods in the Williamson Collection. MA thesis, University of Durham. [Unpublished.]

Quinn P.S. 2022. *Thin section petrography, geochemistry & scanning electron microscopy of archaeological ceramics*. Oxford: Archaeopress.

Schmidt C., Döpper S., Kluge J., Petrella S., Ochs U. ... Walter M. 2021. *Die Entstehung komplexer Siedlungen im Zentraloman Archäologische Untersuchungen zur Siedlungsgeschichte von Al-Khashbah*. Oxford: Archaeopress.

Tite M.S., Freestone I., Mason R., Molera J., Vendrell-Sanz M. & Wood N. 1998. Lead glazes in antiquity — methods of production and reasons for use. *Archaeometry* 40/2: 241–260.

Whitbread I.K. 1995. *Greek transport amphorae, a petrological and archaeological study*. Oxford: The British School at Athens.

Whitbread I.K. 2001. Ceramic petrology, clay geochemistry and ceramic production — from technology to the mind of the potter. Pages 449–459 in D.R. Brothwell & A.M. Pollard (eds), *Handbook of archaeological sciences*. Chichester: John Wiley & Sons.

Whitcomb D. 1975. The archaeology of Oman, a preliminary discussion of the Islamic periods. *The Journal of Oman Studies* 1: 123–157.

Živković J., Carvajal López J.C., Döpper S. & Biezeveld I. 2024. *Bahla ware from Central Oman: Petrological and chemical information on bodies, chemical information on glazes*. DIGITAL.CSIC. doi: https://doi.org/10.20350/digitalCSIC/16704

Živković J., Power T., Georgakopoulou M. & Carvajal López J.C. 2019. Defining new technological traditions of late Islamic Arabia: A view on Bahlā Ware from al-Ain (UAE) and the lead-barium glaze production. *Archaeological and Anthropological Sciences* 11: 4697–4709.

Authors' addresses

Jelena Živković, The Institute of Archaeology, Kneza Mihaila 35/IV, 11000 Belgrade, Serbia; The Cyprus Institute STARC, 20 Konstantinou Kavafi Street, 2121 Nicosia, Cyprus.
e-mail j.zivkovic@ai.ac.rs

José Cristóbal Carvajal López, Institute of Heritage Sciences (INCIPIT) – Spanish Council of Scientific Research (CSIC), Edificio Fontán, Bl. 4, Cidade da Cultura, Monte GAiás s/n 15707 Santiago de Compostela, Spain; School of Archaeology and Ancient History, University of Leicester, University Road, Leicester, LE1 7RH, UK.
e-mail josecristobal.carvajal-lopez@incipit.csic.es

Irini Biezeveld, Drents Museum, Brink 1–5, NL-9400 AC Assen, The Netherlands.
e-mail i.biezeveld@drentsmuseum.nl

Stephanie Döpper, Ancient Near Eastern Studies, University of Würzburg, Residenzplatz 2, Tor A, 97070 Würzburg, Germany.
e-mail stephanie.doepper@uni-wuerzburg.de